A Generalized Multicarrier Communication System – Part III: Dual Symbol Superposition Block Carrier Transmission with Frequency Domain Equalization

Imran Ali

self@ImranAliPhD.com

Independent Researcher, Melbourne, Australia

Abstract

This paper proposes dual symbol superposition block carrier transmission with frequency domain equalization (DSS-FDE) system. This system is based upon χ-transform matrix, which is obtained by concatenation of discrete Hartley transform (DHT) matrix and discrete Fourier transform (DFT) matrices into single matrix that is remarkably sparse, so that, as it will be shown in this paper, it only has non-zero entries on its principal diagonal and one below the principle anti-diagonal, giving it shape of Latin alphabet χ. When multiplied with constellation mapped complex transmit vector, each entry of resultant vector is weighted superposition of only two entries of original vector, as opposed to all entries in conventional DFT based OFDM. Such a transmitter is close to single carrier block transmission with frequency domain equalization (SC-FDE), which is known to have no superposition. The DSS-FDE offers remarkable simplicity in transmitter design and yields great benefits in reduced complexity and low PAPR. At receiver-end, it offers the ability to harvest full diversity from multipath fading channel, full coding gain, with significant bit error rate (BER) improvement. These results will be demonstrated using both analytical expressions, as well as simulation results. As will be seen, this paper is Part III of three-paper series on alternative transforms for multicarrier communication (MC) systems.

Keywords:
OFDM, . Multicarrier Communication System, discrete Hartley transform (DHT), discrete Fourier transform (DFT)

1. Introduction

The conventional orthogonal frequency division multiplexing (OFDM) transmission scheme comes with attractive features as well as some drawbacks. As discussed in detail Part I and Part II in this series, (see [1] and [2]), numerous approaches have been taken to address issues, including some existing work on use of alternative transforms [3]-[5].

In addition to employing the DHT itself as an alternative transform for MC system [[6][7], previous research on precoding OFDM using the DHT transform has been published [8]-[12]. The reduction of PAPR has been demonstrated [8]-[10], whereas analysis or error

performance can be found in the [11]-[12]. It is shown in [12] that the concatenation of DHT and DFT matrices produces a sparse matrix, and it is efficient to implement it as a single transform. A similar observation was made in [11], where more commentary on lowering the transmitter complexity by combining the DHT and DFT into single transform and implementation mechanism is also proposed, along with some error performance.

This paper delves into detail about the structure of the of the matrix that is obtained by the concatenation of DHT and DGT transforms. It will be shown that only the entries on the diagonal and one anti-diagonal below principle anti-diagonal are the only places where it has non-zero entries. When such a matrix is multiplied with a transmission vector containing complex quadrature amplitude modulation (QAM) symbol, each entry in resulting vector is a weighted superposition of only two symbols from original vector. Thus, such a transmission can be classified as dual symbol superposition (DSS). This paper goes much deeper into analysis PAPR of such a transmission, and derives closed form PAPR expression, along with its cumulative distribution function (cdf). At receiver-end, sensitivity to timing synchronization, as well error performance analysis is carried out where it is shown that such a system can harvest full channel diversity and full coding gain. In the following, the contributions of this paper are summarized.

A. Contributions of this Paper

Following is the list of contributions of this paper.

a) Element-wise analysis of the χ-transform matrix, including its structure and therefore its complexity implications are presented.
b) The expression for cdf of PAPR of the DSS frequency domain equalization (DSS-FDE) is derived.
c) Expression for signal to noise ratio (SNR) on the kth subcarrier for the zero-forcing (ZF) and minimum mean squared error (MMSE) receiver is derived.

d) It is shown that DSS-FDE achieves full coding gain and can harvest channel diversity is performed for DSS-FDE system.
e) It is shown that, like conventional OFDM, the DSS-FDE does not incur inter-symbol interference (ISI) penalty when the timing synchronization error is within a certain limit.

The remainder of this paper is organized as follows. In Section 2, the DSS-FDE system is introduced, along with the analysis of χ-transform matrix. Section 3 carries out analysis of PAPR, whereas Section 4 presents BER rate performance analysis. Section 5 discusses the sensitivity to timing synchronization and Section 6 comparison of computational complexity between DSS-FDE and SC-FDE. Section 7 concludes this paper.

2. DSS-FDE System

The DSS-FDE system is shown in Figure 1. At the transmitter, a transform obtained from the concatenation of the DHT and IFFT is used, which is denoted by $\chi^{\mathcal{H}} \triangleq F^{\mathcal{H}} H^{\mathcal{H}} = F^{\mathcal{H}} H$ because $H^{\mathcal{H}} = H$, where H and $H^{\mathcal{H}}$ are the DHT and inverse DHT (IDHT) matrices, respectively. Also, it can be seen that $H^{-1} = H^{\mathcal{H}}$ because H is unitary, such that $HH = H^{\mathcal{H}} H^{\mathcal{H}} = I_{N \times N}$. The inverse of $\chi^{\mathcal{H}}$ is given as $\chi \triangleq HF$. One of the main motivations for this system is that $\chi^{\mathcal{H}}$ and χ are sparse, facilitating low complexity implementation, as well as having a low PAPR at the transmitter. For $N \times N$ sized matrices $\chi^{\mathcal{H}}$ and χ, the proportion of non-zero elements is only $\frac{2(N-1)}{N^2}$, which is 0.007 at $N = 256$.

Furthermore, all the non-zero entries of both χ and $\chi^{\mathcal{H}}$ are strictly on the main diagonal and one anti-diagonal below the main anti-diagonal, so that the structure of two matrices resembles the Greek letter χ (see Equation (3) below). It can be seen from the structure of matrices χ and $\chi^{\mathcal{H}}$ that only $2N + 2$ complex multiplications and $N - 2$ additions will be required to perform the each of the two transforms. Since every row of these matrices contains no more than 2 non-zero entries, this system is referred to in this paper as dual symbol superposition (DSS) block transmission, with $\chi^{\mathcal{H}}$ implemented as one transform as opposed to performing the DHT and IFFT transforms separately.

To derive the structure of matrix $\chi^{\mathcal{H}}$, assume that C and S denote the cosine and sine matrices such that their $(u, v)^{\text{th}}$ entries are given as $[C]_{u,v} = \cos\left(\frac{2\pi}{N} uv\right)$ and $[S]_{u,v} = \sin\left(\frac{2\pi}{N} uv\right)$ respectively, then $CS = O_{N \times N}$ and $C + SS = I_N$. Furthermore, the $(u, v)^{\text{th}}$ entries of DHT and IFFT are given as $[H]_{u,v} = [C]_{u,v} + [S]_{u,v}$ and $[F^{\mathcal{H}}]_{u,v} =$

$[C]_{u,v} + j[S]_{u,v}$. Therefore, the $(u, v)^{\text{th}}$ entry of $\chi^{\mathcal{H}}$ can be obtained as follows

$$\chi^{\mathcal{H}} = (C + jS)(C + S) = CC + CS + jSC + jSS$$
$$= CC + jSS \qquad (\because CS = SC = O_{N \times N}) \qquad (1)$$

From (1), it can be seen that

$$[\chi^{\mathcal{H}}]_{u,v} = \sum_{k=0}^{N-1} \left([C]_{u,k}[C]_{k,v} + j[S]_{u,k}[S]_{k,v} \right)$$

$$= \begin{cases} 1 & \text{when } u = v = m\frac{N}{2} + 1, m \in \{0,1\} \\ \frac{1}{2} + j\frac{1}{2} & \text{when } u = v \neq m\frac{N}{2} + 1, m \in \{0,1\} \\ \frac{1}{2} - j\frac{1}{2} & \text{when } v = N - u, 1 \leq u \leq N - 2 \\ 0 & \text{otherwise.} \end{cases} \qquad (2)$$

As an example, the matrix $\chi^{\mathcal{H}}$ for $N = 8$ is shown below

$$\chi_{8\times 8}^{\mathcal{H}} = \begin{bmatrix} 1 & 0 & 0 & 0 & 0 & 0 & 0 & 0 \\ 0 & \frac{1}{2}+j\frac{1}{2} & 0 & 0 & 0 & 0 & 0 & \frac{1}{2}-j\frac{1}{2} \\ 0 & 0 & \frac{1}{2}+j\frac{1}{2} & 0 & 0 & 0 & \frac{1}{2}-j\frac{1}{2} & 0 \\ 0 & 0 & 0 & \frac{1}{2}+j\frac{1}{2} & 0 & \frac{1}{2}-j\frac{1}{2} & 0 & 0 \\ 0 & 0 & 0 & 0 & 1 & 0 & 0 & 0 \\ 0 & 0 & 0 & \frac{1}{2}-j\frac{1}{2} & 0 & \frac{1}{2}+j\frac{1}{2} & 0 & 0 \\ 0 & 0 & \frac{1}{2}-j\frac{1}{2} & 0 & 0 & 0 & \frac{1}{2}+j\frac{1}{2} & 0 \\ 0 & \frac{1}{2}-j\frac{1}{2} & 0 & 0 & 0 & 0 & 0 & \frac{1}{2}+j\frac{1}{2} \end{bmatrix}$$
$$(3)$$

It should be noted that the product of H and $F^{\mathcal{H}}$ is commutative. This can be seen by substituting the expressions of $F^{\mathcal{H}}$ and H, i.e.,

$$F^{\mathcal{H}} H = (C + jS)(C + S)$$
$$= C + CS + jS + jSS$$
$$= C + jSS, \qquad (\because CS = SC = O_{N \times N}) \qquad (4)$$

and then, we have

$$HF^{\mathcal{H}} = (C + S)(C + jS)$$
$$= C + jC + SC + jSS$$
$$= CC + jSS \qquad (5)$$

Similarly, it can be shown that the product of F and H is commutative.

Figure 1 shows two possible receiver configurations. In the first approach, the χ transform is performed at the receiver, leaving the samples in the Hartley domain, which are then subjected to Hartley domain equalization (HDE). This configuration is referred to DSS-HDE in this paper. In

the second approach, the receiver performs the FFT first, carries out frequency domain equalization (FDE) and then performs DHT, so that this configuration is referred to DSS-FDE.

To see the output of the two receiver configurations, first the received sampled signal is given as

$$\boldsymbol{y} = \boldsymbol{H}_c \boldsymbol{\chi}^{\mathcal{H}} \boldsymbol{X} + \boldsymbol{\eta}, \tag{6}$$

where channel matrix $\boldsymbol{H}_c$ is circulant because of cyclic prefix (CP) insertion and removal. Using the zero-forcing (ZF) equalizer in DSS-HDE configuration, it can be seen that (see also Figure 1(a))

$$\begin{aligned} \boldsymbol{Y} &= \boldsymbol{\chi}\boldsymbol{H}_c\boldsymbol{\chi}^{\mathcal{H}}\boldsymbol{X} + \boldsymbol{\chi}\boldsymbol{\eta} \\ &= \boldsymbol{H}\boldsymbol{F}\boldsymbol{H}_c\boldsymbol{F}^{\mathcal{H}}\boldsymbol{H}\boldsymbol{X} + \boldsymbol{\chi}\boldsymbol{\eta} \\ &= \boldsymbol{H}\boldsymbol{D}\boldsymbol{H} + \boldsymbol{\chi}\boldsymbol{\eta}, \end{aligned} \tag{7}$$

where $\boldsymbol{D} = \boldsymbol{F}\boldsymbol{H}_c\boldsymbol{F}^{\mathcal{H}}$ is used in the last equality. It is easy to see that ZF-HDE is given as, $\boldsymbol{\Omega}_{\text{ZF,HDE}}^{-1} = \boldsymbol{H}\boldsymbol{D}^{-1}\boldsymbol{H}$ and in such case, the estimate of the transmitted vector $\boldsymbol{X}$ is given as

$$\begin{aligned} \hat{\boldsymbol{X}}_{\text{ZF,HDE}} &\triangleq \boldsymbol{\Omega}_{\text{ZF,HDE}}^{-1}\boldsymbol{Y} \\ &= \boldsymbol{H}\boldsymbol{D}^{-1}\boldsymbol{H}\boldsymbol{\chi}\boldsymbol{H}_c\boldsymbol{\chi}^{\mathcal{H}}\boldsymbol{X} + \boldsymbol{H}\boldsymbol{D}^{-1}\boldsymbol{H}\boldsymbol{\chi}\boldsymbol{\eta} \\ &= \boldsymbol{H}\boldsymbol{D}^{-1}\boldsymbol{H}\boldsymbol{H}\boldsymbol{F}\boldsymbol{F}^{\mathcal{H}}\boldsymbol{D}\boldsymbol{F}\boldsymbol{F}^{\mathcal{H}}\boldsymbol{H}\boldsymbol{X} + \boldsymbol{H}\boldsymbol{D}^{-1}\boldsymbol{H}\boldsymbol{H}\boldsymbol{F}\boldsymbol{\eta} \\ &= \boldsymbol{X} + \boldsymbol{H}\boldsymbol{D}^{-1}\boldsymbol{F}\boldsymbol{\eta}, \end{aligned} \tag{8}$$

where third equality in (8) follows by substituting back $\boldsymbol{H}_c = \boldsymbol{F}^{\mathcal{H}}\boldsymbol{D}\boldsymbol{F}$, $\boldsymbol{\chi} = \boldsymbol{H}\boldsymbol{F}$ and $\boldsymbol{\chi}^{\mathcal{H}} = \boldsymbol{F}^{\mathcal{H}}\boldsymbol{H}$.

Similarly, from Figure 1(b), using the ZF equalization in DSS-FDE configuration, the estimate of transmitted vector is

$$\begin{aligned} \hat{\boldsymbol{X}}_{\text{ZF,FDE}} &\triangleq \boldsymbol{H}\boldsymbol{\Omega}_{\text{ZF,FDE}}^{-1}\boldsymbol{F}\boldsymbol{H}_c\boldsymbol{\chi}^{\mathcal{H}}\boldsymbol{X} + \boldsymbol{H}\boldsymbol{\Omega}_{\text{ZF,FDE}}^{-1}\boldsymbol{F}\boldsymbol{\eta} \\ &= \boldsymbol{H}\boldsymbol{D}^{-1}\boldsymbol{F}\boldsymbol{F}^{\mathcal{H}}\boldsymbol{D}\boldsymbol{F}\boldsymbol{F}^{\mathcal{H}}\boldsymbol{H}\boldsymbol{X} + \boldsymbol{H}\boldsymbol{D}^{-1}\boldsymbol{F}\boldsymbol{\eta} \\ &= \boldsymbol{X} + \boldsymbol{H}\boldsymbol{F}\boldsymbol{H}_c^{-1}\boldsymbol{F}^{\mathcal{H}}\boldsymbol{F}\boldsymbol{\eta}, \\ &= \boldsymbol{X} + \boldsymbol{H}\boldsymbol{F}\boldsymbol{F}^{\mathcal{H}}\boldsymbol{D}^{-1}\boldsymbol{F}\boldsymbol{\eta}, \\ &= \boldsymbol{X} + \boldsymbol{H}\boldsymbol{D}^{-1}\boldsymbol{F}\boldsymbol{\eta}, \end{aligned} \tag{9}$$

where $\boldsymbol{\Omega}_{\text{ZF, FDE}}^{-1} = \boldsymbol{D}^{-1}$ is the ZF FDE equalizer and has been used in second equality in (9), $\boldsymbol{D}^{-1} = \boldsymbol{F}\boldsymbol{H}_c^{-1}\boldsymbol{F}^{\mathcal{H}}$ has been used in third equality, and $\boldsymbol{H}_c^{-1} = \boldsymbol{F}^{\mathcal{H}}\boldsymbol{D}^{-1}\boldsymbol{F}$ has been used in final equality.

It can be seen that, for the ZF equalizer, the two systems in Figure (a) and (b) have identical estimate of transmitted vector and will match in error performance. Therefore, in the remainder of the paper, only DSS-FDE will be mentioned because it has slightly less complexity.

In particular, since the DHT and DFT are implemented at same complexity [40] and the DSS-HDE performs one extra χ transform, it has extra $2N - 2$ multiplications and $N - 2$ additions. Furthermore, when compared to the conventional OFDM and SC-FDE, the DSS-FDE performs one extra $\chi^{\mathcal{H}}$ transform, so has same amount of extra complexity.

(a) Receiver configuration with Hartley domain equalization

(b) Receiver configuration with single-tap frequency domain equalization
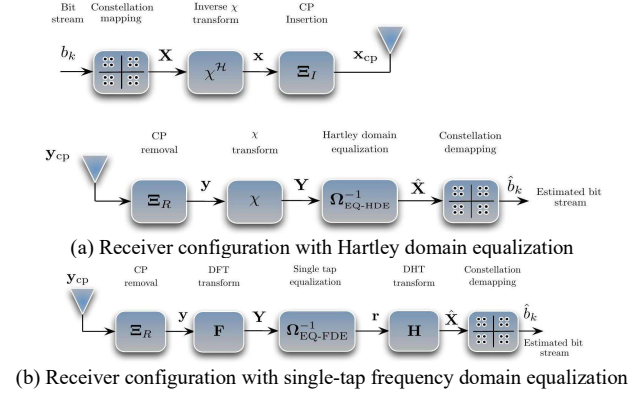
Figure 1: Transmitter of DSS-FDE system with two different receiver configurations

However, the DSS-FDE matches SC-FDE in error performance as will be demonstrated in Section 4 by deriving both the SNR on the kth subchannel of DSS-FDE as well as diversity order and coding gain achieved by it.

3. PAPR of DSS-FDE System

Since $\chi^{\mathcal{H}}$ is a sparse matrix, it has a low PAPR. The expression for the PAPR and its cdf are derived in this section. Recalling the PAPR of GMC in *Theorem 1* of [1], and substituting $\boldsymbol{Q}_T = \chi^{\mathcal{H}}$, the PAPR of DSS-FDE can be written as,

$$\gamma^{\text{DSS-FDE}} = \frac{A_{\max}^2}{2}\max_n\left\{\left|\sum_{m=0}^{N-1} g[\chi^{\mathcal{H}}]_{n,m}\right|^2\right\} \tag{10}$$

where $g \in \{\pm 1 \pm j\}$.

It can be seen from Equation (1) that the first and $\left(\frac{N}{2} + 1\right)^{\text{th}}$ rows have only one non-zero entry, which is 1. Therefore, the PAPR on these subchannels will be $A_{\max}^2$. However, all the remaining rows contain both $\frac{1}{2} + j\frac{1}{2}$ and $\frac{1}{2} - j\frac{1}{2}$ as their only non-zero entries and, using Equation (10), the PAPR on these subchannel can found by finding the maximum across all the possible combinations of $\pm 1 \pm j$. Therefore, it can be seen that,

$$\gamma_{n \neq 0, \frac{N}{2}-1}^{\text{DSS-FDE}} = \frac{A_{\max}^2}{2}\max_{\pm}\left\{\left|\pm\left(\frac{1}{2} + j\frac{1}{2}\right) \pm j\left(\frac{1}{2} + j\frac{1}{2}\right)\right.\right.$$
$$\left.\left. \pm\left(\frac{1}{2} - j\frac{1}{2}\right) \pm j\left(\frac{1}{2} - j\frac{1}{2}\right)\right|^2\right\} \tag{11}$$

with a total of 16 possible sign combinations, regardless of value of N or constellation size M. Through an rigorous exercise of going through these 16 combinations to find the maximum, it can be verified that the maximum of Equation (11) is 4 and therefore the PAPR of DSS-FDE is

$$\gamma^{\text{DSS-FDE}} = 2A_{\max}^2, \tag{12}$$

which is twice the PAPR of single carrier SC-FDE system (lowest possible) but still $\frac{N}{2}$ times lower than that of conventional OFDM.

3.1. CDF of the PAPR of DSS-FDE System

The PAPR expression is tends to be a pessimistic view of PAPR problem because it is theoretical maximum, and it may not occur very often. In order for the maximum PAPR to occur, all subchannel in MC system should be carrying certain maximum power quadrature amplitude modulation (QAM) symbols. Naturally, the probability of this happening decreases with increase in N [13]. Since the PAPR is inherently a probabilistic phenomenon, another more insightful way of looking at it is finding the cdf. The cdf is calculated from the instantaneous PAPR because the value of PAPR at any point depends on the combination of QAM symbols in the current MC symbol.

In the following, the cdf of DSS-FDE is derived. This derivation follows the well-known approach used for the derivation of cdf of zero-padded single carrier system [14]. If $\boldsymbol{x}_{\text{cp}}$ is the vector after inserting cyclic prefix into vector $\boldsymbol{\chi}^{\mathcal{H}}\boldsymbol{X}$, the instantaneous PAPR for DSS-FDE is

$$\gamma_i^{\text{DSS-FDE}} \triangleq \frac{\max_n\left\{\left|\left[\boldsymbol{x}_{\text{cp},i}\right]_n\right|^2\right\}}{\frac{1}{N+L_P}E\|\boldsymbol{x}_{\text{cp},i}\|^2} \tag{13}$$

then the probability that PAPR will exceed a threshold value, γ^{TH}, is given as

$$\Pr\left(\gamma_i^{\text{DSS-FDE}} > \gamma^{\text{TH}}\right) = \Pr\left(\frac{\max_n\left\{\left|\left[\boldsymbol{x}_{\text{cp},i}\right]_n\right|^2\right\}}{\frac{1}{N+L_P}E\|\boldsymbol{x}_{\text{cp},i}\|^2} > \gamma^{\text{TH}}\right)$$
$$= \Pr\left(\max_n\left\{\left|\left[\boldsymbol{x}_{cp,i}\right]_n\right|^2\right\} > \frac{\gamma^{TH}}{N+L_P}E\|\boldsymbol{x}_{cp,i}\|^2\right) \tag{14}$$

It can be seen that maximum will not change before and after the insertion of cyclic, i.e., $\max_n\left\{\left|\left[\boldsymbol{x}_{\text{cp},i}\right]_n\right|^2\right\} = \max_n\{|[\boldsymbol{x}_i]_n|^2\}$ and $\frac{1}{N+L_P}E\|\boldsymbol{x}_{\text{cp},i}\|^2 = \frac{1}{N}E\|\boldsymbol{x}_i\|^2$, so then

$$\Pr\left(\gamma_i^{\text{DSS-FDE}} > \gamma^{\text{TH}}\right) = \Pr\left(\max_n\{|[\boldsymbol{x}_i]_n|^2\} > \frac{\gamma^{\text{TH}}}{N}E\|\boldsymbol{x}_i\|^2\right)$$
$$= \Pr\left(\max_n\{|[\boldsymbol{x}_i]_n|\} > \sqrt{\frac{\gamma^{\text{TH}}}{N}E\|\boldsymbol{x}_i\|^2}\right)$$
$$= \Pr\left(\max_n\{|[\boldsymbol{x}_i]_n|\} > \sqrt{\gamma^{TH}E\{|[\boldsymbol{x}_i]_n|^2\}}\right)$$
$$= 1 - \Pr\left(\max_n\{|[\boldsymbol{x}_i]_n|\} \le \sqrt{\gamma^{TH}E\{|[\boldsymbol{x}_i]_n|^2\}}\right) \tag{15}$$

Under the assumption that the symbols are independent and identically distributed (i.i.d.), they are drawn uniformly from the QAM constellation alphabet, $\mathcal{A}$. Therefore, $[\boldsymbol{x}_i]_n, \forall i, n$ are also i.i.d. distributed but do not necessarily follow a uniform distribution (the distribution of $[\boldsymbol{x}_i]_n$ for DSS transmission will be derived shortly as it is needed for cdf). Therefore, it can be written from Equation (15) that

$$\Pr\left(\gamma_i^{\text{DSS-FDE}} > \gamma^{\text{TH}}\right) = 1 - \prod_{n=0}^{N-1}\left(\Pr\left(|[\boldsymbol{x}_i]_n| \le \sqrt{\gamma^{TH}E\{|[\boldsymbol{x}_i]_n|^2\}}\right)\right)$$
$$= 1 - \left(\Pr\left(|[\boldsymbol{x}_i]_n| \le \sqrt{\gamma^{TH}E\{|[\boldsymbol{x}_i]_n|^2\}}\right)\right)^N \tag{16}$$

where again the i.i.d. nature of $[\boldsymbol{x}_i]_n, \forall i, n$, is utilized.

To evaluate $E\{|[\boldsymbol{x}_i]_n|^2\}$, the probability distribution of $[\boldsymbol{x}_i]_n, \forall n$, needs to be known, which will be derived from distribution of $[\boldsymbol{X}_i]_n \in \mathcal{A}$. In particular, to find the distributions of $\Re\{[\boldsymbol{X}_i]_n\}$ and $\Im\{[\boldsymbol{X}_i]_n\}$, where $\Re\{.\}$ and $\Im\{.\}$ are respectively the real and imaginary parts of the argument, notice that they are uniformly distributed between $\frac{A_{\max}}{\sqrt{2}}$ and $-\frac{A_{\max}}{\sqrt{2}}$, so that their distribution is $\frac{1}{(A_{\max}/\sqrt{2})-(-A_{\max}/\sqrt{2})} = \frac{1}{\sqrt{2}A_{\max}}$, the pdfs of $\Re\{[\boldsymbol{x}_i]_n\}$, for large M, i.e., [6]

$$f_{\Re\{[\boldsymbol{x}_i]_n\}} = f_{\Im\{[\boldsymbol{x}_i]_n\}}$$
$$\sim \begin{cases} \frac{1}{\sqrt{2}A_{\max}} & \Re\{[\boldsymbol{X}]_n\} \le \frac{A_{\max}}{\sqrt{2}}, \Im\{[\boldsymbol{X}]_n\} \le \frac{A_{\max}}{\sqrt{2}} \\ 0 & \text{otherwise} \end{cases} \tag{17}$$

To express $[\boldsymbol{x}_i]_n$ as a function of $\Re\{[\boldsymbol{X}_i]_n\}$ and $\Im\{[\boldsymbol{X}_i]_n\}$, use the structure of matrix $\boldsymbol{\chi}$ in the Equation (2), so that the nth entry of $[\boldsymbol{x}_i]_n$ can now be written as

$$[\boldsymbol{x}_i]_n = \sum_{k=0}^{N-1}[\boldsymbol{\chi}]_{n,k}[\boldsymbol{X}_i]_k$$
$$= \begin{cases} \left(\frac{1}{2}+j\frac{1}{2}\right)[\boldsymbol{X}_i]_n & n=0 \text{ or } n=\frac{N}{2} \\ \left(\frac{1}{2}+j\frac{1}{2}\right)[\boldsymbol{X}_i]_n + \left(\frac{1}{2}-j\frac{1}{2}\right)[\boldsymbol{X}_i]_{N-n} & \text{otherwise} \end{cases} \tag{18}$$

Then, after some simple modifications, the real and imaginary parts of $[\boldsymbol{x}_i]_n$ can be written respectively as

$\Re\{[\boldsymbol{x}]_i]_n\}$
$$= \begin{cases} \frac{1}{2}(\Re\{[\boldsymbol{X}_i]_n\} - \Im\{[\boldsymbol{X}_i]_n\}) & n = 0 \text{ or } n = \frac{N}{2} \\ \frac{1}{2}(\Re\{[\boldsymbol{X}_i]_n + [\boldsymbol{X}_i]_{N-n} + \Im\{[\boldsymbol{X}_i]_{N-n} - [\boldsymbol{X}_i]_n\}) & \text{otherwise} \end{cases}$$
(19)

$\Im\{[\boldsymbol{x}]_i]_n\}$
$$= \begin{cases} \frac{1}{2}(\Re\{[\boldsymbol{X}_i]_n\} + \Im\{[\boldsymbol{X}_i]_n\}) & n = 0 \text{ or } n = \frac{N}{2} \\ \frac{1}{2}(\Re\{[\boldsymbol{X}_i]_n - [\boldsymbol{X}_i]_{N-n}\} + \Im\{[\boldsymbol{X}_i]_{N-n} + [\boldsymbol{X}_i]_n\}) & \text{otherwise} \end{cases}$$
(20)

Since the pdf of sum of two mutually independent random variables U and V, with individual pdf's $f_U(x)$ and $f_V(x)$ respectively, is given as [15]

$$f_{U+V}(x) = \int_{-\infty}^{+\infty} f_U(x) f_Y(x-y) dy \qquad (21)$$

the pdf's of both $\frac{1}{2}(\Re\{[\boldsymbol{X}_i]_n\} \pm \Im\{[\boldsymbol{X}_i]_n\}), n = 0$ or $n = \frac{N}{2}$, is given as

$$f_{\frac{1}{2}(\Re\{[X_i]_n\}\pm\Im\{[X_i]_n\})}(x) \sim \frac{1}{2} \cdot \frac{1}{\sqrt{2}A_{\max}} \cdot \frac{1}{\sqrt{2}A_{\max}} \int_{-\frac{A_{\max}}{\sqrt{2}}}^{+\frac{A_{\max}}{\sqrt{2}}} 1 dy$$

$$\sim \begin{cases} \frac{1}{2A_{\max}^2} & \Re\{[X]_n\} \le \frac{A_{\max}}{\sqrt{2}}, \Im\{[X]_n\} \le \frac{A_{\max}}{\sqrt{2}} \\ 0 & \text{otherwise} \end{cases}$$
(22)

Similarly, both $\Re\{[\boldsymbol{X}_i]_n \pm [\boldsymbol{X}_i]_{N-n}\}$ and $\Im\{[\boldsymbol{X}_i]_{N-n} \pm [\boldsymbol{X}_i]_n\}$ are uniformly distributed between $\sqrt{2}A_{\max}$ and 0, therefore,

$$f_{\frac{1}{2}(\Re\Re\{[X_i]_n\pm[X_i]_{N-n}\})+\frac{1}{2}(\Im\{[X_i]_{N-n}\pm[X_i]_n\})}(x)$$

$$\sim \frac{1}{2} \cdot \frac{1}{\sqrt{2}A_{\max}} \cdot \frac{1}{\sqrt{2}A_{\max}} \int_{-\frac{A_{\max}}{\sqrt{2}}}^{+\frac{A_{\max}^{\sqrt{2}}}{\sqrt{2}}} 1 dy$$

$$\sim \begin{cases} \frac{1}{2A_{\max}^2} & \Re\{[s]_n\} \le \frac{A_{\max}}{\sqrt{2}}, \Im\{[s]_n\} \le \frac{A_{\max}}{\sqrt{2}} \\ 0 & \text{otherwise} \end{cases}$$
(23)

which is identical to that of $\frac{1}{2}(\Re\{[\boldsymbol{X}_i]_n\} \pm \Im\{[\boldsymbol{X}_i]_n\})$. Therefore, the pdf's of real and imaginary parts n^{th} element of DSS-DCE symbol, $[\boldsymbol{x}_i]_n$ can be written as,

$$f_{\Re\{[x_i]_n\}} = f_{\Im\{[x_i]_n\}}$$
$$\sim \begin{cases} \frac{1}{2A_{\max}^2} & \Re\{[X]_n\} \le \frac{A_{\max}}{\sqrt{2}}, \Im\{[X]_n\} \le \frac{A_{\max}}{\sqrt{2}} \\ 0 & \text{otherwise} \end{cases}$$
(24)

From the pdfs of real and imaginary parts can be combine into the pdf of $[\boldsymbol{x}_i]_n$ by

$$f_{[x_i]_n} \sim \frac{1}{2} \cdot \frac{1}{2A_{\max}^2} \cdot \frac{1}{2A_{\max}^2} \int_{-\frac{A_{\max}}{\sqrt{2}}}^{+\frac{A_{\max}}{\sqrt{2}}} 1 dy$$

$$\sim \begin{cases} \frac{1}{(\sqrt{2}A_{\max})^3} & \Re\{[X]_n\} \le \frac{A_{\max}}{\sqrt{2}}, \Im\{[X]_n\} \le \frac{A_{\max}}{\sqrt{2}} \\ 0 & \text{otherwise} \end{cases}$$
(25)

Now returning to computation of $E\|[\boldsymbol{x}_i]_n\|^2$, let $y \triangleq \Re\{[\boldsymbol{x}_i]_n\}$ and $z \triangleq \Im\{[\boldsymbol{x}_i]_n\}$, it can be written that,

$$E\|[\boldsymbol{x}_i]_n\|^2 = \frac{1}{(\sqrt{2}A_{\max})^3} \int_{-\frac{A_{\max}}{\sqrt{2}}}^{+\frac{A_{\max}}{\sqrt{2}}} \int_{-\frac{A_{\max}}{\sqrt{2}}}^{\sqrt{2}} (y^2 + z^2) dy dz$$

$$= \frac{1}{2\sqrt{2}A_{\max}^3} \int_{-\frac{A_{\max}}{\sqrt{2}}}^{\sqrt{2}} \left(\frac{A_{\max}^3}{3\sqrt{2}} + \sqrt{2}A_{\max}z^2\right) dz$$

$$= \frac{1}{2\sqrt{2}A_{\max}^3} \cdot \frac{2A_{\max}^4}{3}$$

$$= \frac{1}{3\sqrt{2}}A_{\max}.$$
(26)

Therefore, the cdf of DSS-FDE can be written as,

$$\Pr\left(\gamma_i^{\text{DSS-FDE}} > \gamma^{\text{TH}}\right) = 1 - \left(\Pr\left(|[\boldsymbol{x}_i]_n| \le \sqrt{\gamma^{\text{TH}}\frac{A_{\max}}{3\sqrt{2}}}\right)\right)^N.$$
(27)

Figure 2 compares the cdf of OFDM, T-OFDM, SC-FDE and DSS-FDE systems at $N = 256$. The results are obtained over 1000 simulation runs. As can be seen the curves drop very sharply from 10^0 to 10^{-6} for SC-FDE and DSS-FDE at around 3 dB and 6 dB respectively. This can be interpreted as almost 100% probability the PAPR will below 3 or 6 dB respectively for DSS-FDE and DSS-FDE and highly unlikely that it will go beyond those points.

4. Error Performance Analysis

From Equation (32) in [1], which gives expression for the SNR on k^{th} subchannel of the GMC system with ZF equalization, the SNR on the kth subchannel of DSS-FDE with ZF equalization can be obtained by putting $\boldsymbol{Q}_R = \boldsymbol{\chi}$, i.e.,

$$\beta_k^{\text{ZF,DSS-F}}$$

$$= \beta_o \cdot \frac{\prod_{n=0}^{N-1} |[\boldsymbol{D}]_{n,n}|^2}{\sum_{n=0}^{N-1} |[\boldsymbol{\chi}\boldsymbol{F}^{\mathcal{H}}]_{k,n}|^2 \prod_{m=0,m\neq n}^{N-1} |[\boldsymbol{D}]_{m,m}|^2}$$

$$= \beta_o \cdot \frac{\prod_{n=0}^{N-1} |[\boldsymbol{D}]_{n,n}|^2}{\sum_{n=0}^{N-1} |[\boldsymbol{H}]_{k,n}|^2 \prod_{m=0,m\neq n}^{N-1} |[\boldsymbol{D}]_{m,m}|^2},$$
(28)

where $\boldsymbol{\chi}\boldsymbol{F}^{\mathcal{H}} = \boldsymbol{F}\boldsymbol{H}\boldsymbol{F}^{\mathcal{H}} = \boldsymbol{H}\boldsymbol{F}\boldsymbol{F}^{\mathcal{H}} = \boldsymbol{H}$ has been used in the second equality.

Recall that $\beta_o = \frac{1}{N_o}$ is the additive white Gaussian noise (AWGN) channel SNR for a normalized modulation constellation. After dividing both numerator and denominator by $\prod_{n=0}^{N-1} |[D]_{n,n}|^2$, the relationship between the ZF SNR of conventional OFDM and DSS-FDE can be found as

$$\beta_k^{\text{ZF,DSS-F}} = \frac{1}{\sum_{n=0}^{N-1} \frac{|[H]_{k,n}|^2}{\beta_o |[D]_{n,n}|^2}}$$

$$= \frac{1}{\sum_{n=0}^{N-1} \frac{|[H]_{k,n}|^2}{\beta_n^{Z\,F,\,\text{OFDM}}}}. \tag{29}$$

By definition,

$$|[H]_{k,n}|^2 = \frac{1}{N} \left([C]_{k,n} + [S]_{k,n} \right) \left([C]_{k,n} + [S]_{k,n} \right)^{\mathcal{H}}$$

$$= \frac{1}{N} \left(\cos^2 \left(\frac{2\pi}{N} kn \right) + \sin^2 \left(\frac{2\pi}{N} kn \right) + 2\cos \left(\frac{2\pi}{N} kn \right) \sin \left(\frac{2\pi}{N} kn \right) \right)$$

$$= \frac{1}{N} \left(1 + 2\cos \left(\frac{2\pi}{N} kn \right) \sin \left(\frac{2\pi}{N} kn \right) \right)$$

$$= \frac{1}{N} \left(1 + \sin \left(2\frac{2\pi}{N} kn \right) \right), \tag{30}$$

where in third equality in (30) the identity $\cos^2 \alpha + \sin^2 \alpha = 1$ and in last equality, expression $\cos (\alpha)\sin (\beta) = \frac{1}{2} \sin (\alpha + \beta)$ have been used [16].

Since $\sin \left(2\frac{2\pi}{N} kn \right)$ does not have a constant envelope, $|[H]_{k,n}|^2 \neq |[H]_{k',n'}|^2$ for $k \neq k', n \neq n'$, which leads to the observation that the ZF equalized SNR on all the subchannels of DSS-FDE are not the same. For comparison, that it is same for all subchannels of SC-FDE [17]. However, the SNR distribution for different subchannels of DSS-FDE is still not completely random. To see this, use the value of $|[H]_{k,m}|^2$ from Equation (30) in Equation (28) to get

$$\beta_k^{\text{ZF,DSS-FDE}} = \frac{1}{\frac{1}{N} \sum_{n=0}^{N-1} \frac{1 + \sin \left(2\frac{2\pi}{N} kn \right)}{\beta_o |[D]_{n,n}|^2}}$$

$$= \frac{1}{\frac{1}{N} \sum_{n=0}^{N-1} \frac{1}{\beta_o |[D]_{n,n}|^2} + \frac{1}{N} \sum_{n=0}^{N-1} \frac{\sin \left(2\frac{2\pi}{N} kn \right)}{\beta_o |[D]_{n,n}|^2}} \tag{31}$$

From Equation (34) in [1], it can be seen that the first summation in the denominator of Equation (31) is $1/\beta^{\text{ZF, SC-FDE}}$. Furthermore, define

$$\mu_k \triangleq \frac{1}{N} \sum_{n=0}^{N-1} \frac{1}{|[D]_{n,n}|^2} \sin \left(2\frac{2\pi}{N} kn \right) \tag{32}$$

After substituting the value of μ_k in Equation (31),

$$\beta_k^{\text{ZF,DSS-F}} = \frac{1}{\frac{1}{\beta_{\text{ZF,SC-FD}}} + \frac{\mu_k}{\beta_o}} = \frac{\beta_o \beta^{\text{ZF,SC-FD}}}{\beta_o + \mu_k \beta^{\text{ZF,SC-FD}}} \tag{33}$$
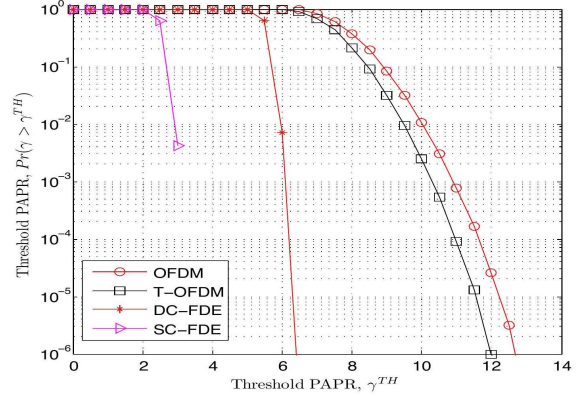

Figure 2: The CDF of PAPR of different system at $N = 256$

It is important to notice here that, since the μ_k involves weighted average of all subchannel responses, $[D]_{n,n}, \forall n$, the dependence of μ_k on the channel response matrix D is the same for all k and any variation in μ_k is the result of variation in the sinusoidal terms that depend on k. Therefore, Equation (33) suggests that the relationship between the SNRs on the kth and k'^{th} subchannel is strictly the function of k and k' regardless of channel conditions. This can be compared with the the SC-FDE, which has the same SNR on all subchannels regardless of the channel conditions for each subchannel and hence precoding with FFT is referred to as channel independent precoding [18]. While the SNR on the kth subchannels of DSS-FDE is not the same for all k, it is still independent of channel conditions on k^{th} subchannel, $[D]_{k,k}$, so that precoding with DHT is also channel indepdent precoding. The authors in [5] suggest channel independent precoding is achieved when, for an $N \times N$ precoding matrix U, $|[U]_{u,v}| = \frac{1}{\sqrt{N}}$ for all u, v. Although $|[H]_{u,v}| \neq \frac{1}{\sqrt{N}}, \forall u, v$, the DHT matrix, H, is still a channel independent precoding.

To elaborate this idea further, refer to Equation (33), which not only shows the relationship between SNRs of SC-FDE and DSS-FDE on the kth subchannel when ZF equalization is used, it also provides some interesting insights into DSS-FDE system performance, as will be seen shortly. The SNR comparison between SC-FDE and DSS-FDE is dictated by the parameter μ_k and therefore, by k. In particular,

$$\beta_k^{\text{ZF,DSS−FDE}} \begin{cases} > \beta^{\text{ZF,SC−FDE}} & \text{if } \mu_k < 0 \\ = \beta^{\text{ZF,SC−FDE}} & \text{if } \mu_k = 0 \\ < \beta^{\text{ZF,SC−FDE}} & \text{if } \mu_k > 0 \end{cases} \quad (34)$$

Using a numerical exercise for any realization of diagonal channel response matrix, D, over all $0 \le k \le N − 1$, it can be easily checked that, when $N \ge 4$, for every μ_k there exists a unique $\mu_{k'}$ such that $\mu_k + \mu_{k'} = 0, \forall k \ne k'$, because

$$\mu_{\frac{pN}{4}} = 0 = −\mu_{\frac{pN}{4}} \text{ for } 0 \le p \le \frac{N}{4} − 1$$

$$\mu_p = −\mu_{\frac{N}{2}−p} \text{ for } 1 \le p \le \frac{N}{4} − 1 \quad (35)$$

$$\mu_{\frac{N}{2}+p} = −\mu_{N−p} \text{ for } 1 \le p \le \frac{N}{4} − 1$$

By using the observations in Equation (34) in Equation (33), it can be shown that, for every k for which $\beta^{\text{ZF,SC−FDE}} − \beta_k^{\text{ZF,DSS−F}} = \Delta$, there exists a unique k' such that $\beta^{\text{ZF,SC−FDE}} − \beta_{k'}^{\text{ZF,DSS−FDE}} = −\Delta$. Thus, on k^{th} subchannel, if the SNR of SC-FDE is higher than DSS-FDE by a certain margin Δ, then there necessarily exists k' such that the SNR of DSS-FDE on k' th subchannel is higher than SC-FDE by same Δ. This observation can be formalized as follows:

Observation 1:

1) In given channel conditions, the average SNR of a DSS-FDE symbol is same as that of SC-FDE, i.e.,

$$\frac{1}{N} \sum_{k=0}^{N−1} \beta_k^{\text{ZF,DSS−F}} = \beta^{\text{ZF,SC−FDE}} \quad (36)$$

and since error performance is average of all subchannels, both systems have same performance (see simulation graphs in Figure 3). Notice that average is taken over subchannels within a symbol, not over more than one symbols.

2) Conventional OFDM is known to suffer BER loss compared to SC-FDE in frequency selective channels due to deeply faded low SNR subcarriers, however, unlike DSS-FDE, there isn't necessarily a correspondingly high SNR subcarrier to average out the BER loss.

3) Furthermore, it has been suggested in the literature (see [5], discussion after Theorem 1) that precoding matrices, U, for which $|[U]_{u,v}| = \frac{1}{\sqrt{N}}, \forall u, v$, are channel independent and hence optimal precoders in terms of BER performance. From the analysis in this section, it has been shown that, while there exist u and v for which $|[H]_{u,v}|^2 \ne \frac{1}{N}$, the matrix H is still a channel independent precoder and DSS-FDE matches error performance SC-FDE.

Figure 3 shows simulation results to compare the BER performance of DSS-FDE with SC-FDE, T-OFDM and the conventional OFDM. In all simulations, all transforms have dimension of $N = 256$ and 16-QAM modulated symbols are transmitted across a Rayleigh fading channel which is modeled by a Stanford University Interim (SUI)-5 [19] type three-path channel with propagation delays and fading margins of $[0\ 4\ 10]\mu s$ and $[0 − 5 − 10]$dB respectively.
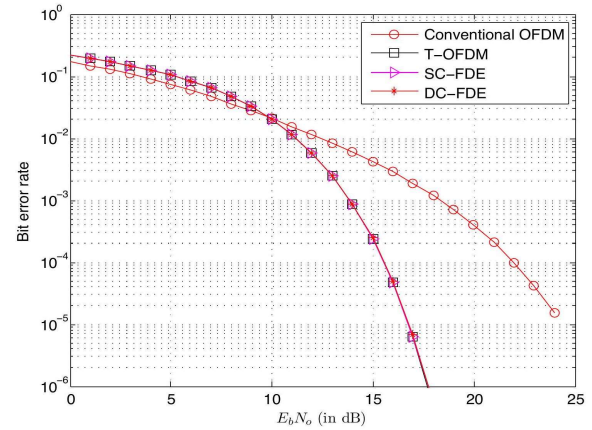

Figure 3: The BER performance comparison of different systems

The channel response is assumed to remain constant for the duration of one MC symbol and the BER graphs were averaged over 1000 simulations runs. As can be seen, the DHT precoded system, T-OFDM and SC-FDE offer substantial BER performance gain over conventional OFDM. Specifically, at a BER of $10^{−5}$, approximately 7 dB gain is observed for these otherwise uncoded systems.

5. Timing Synchronisation Performance

In *Theorem 2* of the [1], the conditions over GMC system based upon generalized $Q_T \mid Q_R$ transform pair, which would lead to identical performance to that of conventional OFDM due to timing error, ζ, when it holds the bound $L_P − L \le \zeta \le 0$ were identified in and these are:

a) Q_R is N-periodic and $[Q]_{u,v+\zeta} = g(K_u, [Q]_{u,v})$, where K_u is independent of v but same for all entries of uth row, and $g(\cdot, \cdot)$ is an arithmetic operation between the arguments, or

b) the Q_R itself does not satisfy condition (a) but it can be expressed as $Q_R = \tilde{Q}_R \Psi$, where $\tilde{Q}_R$ satisfies condition (a) and Ψ is N-periodic.

To see the applicability of this theorem to the transform matrix $\chi = HF$, first it should be checked if χ is periodic. It was shown in [1] *Lemma 2*, that product of two N-periodic matrices is also N-periodic. The matrix F is already well-known to be N-periodic. To check the periodicity of H, its $(u, v)^{\text{th}}$ entry is given as

$$[\boldsymbol{H}]_{u,v} = \frac{1}{\sqrt{N}}\left(\cos\left(\frac{2\pi}{N}uv\right) + \sin\left(\frac{2\pi}{N}uv\right)\right)$$

$$\Rightarrow [\boldsymbol{H}]_{u,v+p} = \frac{1}{\sqrt{N}}\left(\cos\left(\frac{2\pi}{N}u(v+pN)\right) + \sin\left(\frac{2\pi}{N}u(v+pN)\right)\right)$$

$$= \frac{1}{\sqrt{N}}\left(\cos\left(\frac{2\pi}{N}uv + 2\pi pu\right) + \sin\left(\frac{2\pi}{N}uv + 2\pi pv\right)\right)$$

$$= [\boldsymbol{H}]_{u,v}. \qquad (37)$$

Using similar method, it can be shown that $[\boldsymbol{H}]_{u+qN,v} = [\boldsymbol{H}]_{u,v}$, so it can be said that $\boldsymbol{H}$ is N-periodic. Since $\boldsymbol{H}$ is periodic and the product of $\boldsymbol{H}$ and $\boldsymbol{F}$ is commutative, i.e., $\boldsymbol{\chi} = \boldsymbol{HF} = \boldsymbol{FH}$ (see Section 2), by letting $\boldsymbol{Q}'_R = \boldsymbol{F}$, the matrix $\boldsymbol{\chi}$ satisfies the part **(b)** of theorem because $\boldsymbol{F}$ satisfies part **(a)**. Therefore, DSS-FDE system will incur only a phase offset when the timing error is in range $L_P - L \le \zeta \le 0$, regardless of whether FDE or HDE equalization is used. This should be compared with T-OFDM, where it was seen that since $\boldsymbol{WF} \ne \boldsymbol{FW}$, there will be interference whenever T-transform is implemented at receiver as one transform and $\zeta \ne 0$. Thus, DSS-FDE is less sensitive to timing errors than dyadic convolution-based T-OFDM [20].

6. Complexity Comparison of DSS-FDE and SC-FDE

When time domain signal generation is used, the SC-FDE transmitter does not need to compute any transforms and hence it only uses CP insertion. In case of DSS-FDE, a total of $N - 2$ additions and $N - 2$ multiplications will be needed to execute $\chi^{\mathcal{H}}$-transform. At the receiver, both systems compute two transforms of the same complexity, $N\log_2 N$ additions and multiplications and single tap equalization of N multiplications. Thus, baseband SC-FDE has a total $N + N\log_2 N$ multiplications and $N\log_2 N$ additions in comparison to DSS-FDE, which has $2N - 2 + N\log_2 N$ multiplications and $N - 2 + N\log_2 N$ additions. Therefore, DSS-FDE has slightly higher complexity for time domain signal generation.

However, it has been suggested in, for example [21], that frequency domain signal generation, although equivalent, is more bandwidth efficient due to improved filtering in the frequency domain. This comes at the cost of performing both transforms at the transmitter as well. The long-term evolution (LTE) standard allows both time domain and frequency domain methods of signal generation [22]. In frequency domain signal generation, the complexity of two systems will be identical.

7. Conclusions

This paper studied the DSS-FDE system in detail, as well explored the structure of the χ-transform matrix, and resulting implication on PAPR and computation complexity. It was shown analytically that DSS-FDE has twice the PAPR of single carrier system but still half that of conventional OFDM. Furthermore, the paper showed that, much like conventional OFDM, when timing synchronization is less than the length of cyclic prefix, the DSS-FDE system does not incur any BER performance penalty. The SNR on the given subchannel was also studied, along the ability of DSS-FDE system to harvest channel diversity and achieve full coding gain. These were also corroborated with simulation results.

References

[1] Ali, I. "A Generalized Multicarrier Communication System—Part I: Theoretical Performance Analysis and Bounds." *International Journal of Computer Science and Network Security* 24, no. 9 (2024): 1–11

[2] Ali, I. "A Generalized Multicarrier Communication System—Part II: The T-OFDM System." *International Journal of Computer Science and Network Security* 24, no. 9 (2024): 21–29

[3] Ahmed, M. S., S. Boussakta, B. Sharif, and C. C. Tsimenidis. "OFDM Based on Low Complexity Transform to Increase Multipath Resilience and Reduce PAPR." *IEEE Transactions on Signal Processing* 59, no. 12 (2011): 5994–6007.

[4] Ali, I., A. Pollok, L. Luo, and L. Davis. "A Low Complexity Receiver for T-Transform Based OFDM Systems." In *Proceedings of IEEE 22nd International Symposium on Personal Indoor and Mobile Radio Communications*, 1611–1615. Toronto, Canada, 2011.

[5] Ahmed, M., S. Boussakta, B. Sharif, and C. Tsimenidis. "OFDM Based New Transform with BER Performance Improvement Across Multipath Transmission." In *Proceedings of IEEE International Conference on Communications*, 1–5. Cape Town, South Africa, May 2010.

[6] Wang, D., D. Liu, F. Liu, and G. Yue. "A Novel DHT-Based Ultra-Wideband System." In *Proceedings of IEEE International Symposium on Communications and Information Technology*, 672–675. Beijing, China, October 2005.

[7] Jao, C., S. Long, and M. Shiue. "DHT-Based OFDM System for Passband Transmission Over Frequency-Selective Channel." *IEEE Signal Processing Letters* 17, no. 8 (2010): 699–702.

[8] Baig, I., and V. Jeoti. "PAPR Analysis of DHT-Precoded OFDM System for M-QAM." In *International Conference on Intelligent and Advanced Systems (ICIAS)*, 1–4. Kuala Lumpur, Malaysia, June 15–17, 2010.

[9] Sharifi, A. A. "Discrete Hartley Matrix Transform Precoding-Based OFDM System to Reduce the High PAPR." *ICT Express* 5, no. 2 (2019): 100–103.

[10] Baig, I., U. Farooq, N. U. Hasan, M. Zghaibeh, A. Sajid, and U. M. Rana. "A Low PAPR DHT Precoding Based UFMC

Scheme for 5G Communication Systems." In *2019 6th International Conference on Control, Decision and Information Technologies (CoDIT)*, 425–428. Paris, France, April 2019.

[11] Ouyang, X., J. Jin, G. Jin, and P. Li. "Low Complexity Discrete Hartley Transform Precoded OFDM System Over Frequency-Selective Fading Channel." *ETRI Journal* 37, no. 1 (2015): 32–42.

[12] Anoh, K., C. Tanriover, M. V. Ribeiro, B. Adebisi, and C. H. See. "On the Fast DHT Precoding of OFDM Signals Over Frequency-Selective Fading Channels for Wireless Applications." *Electronics* 11, no. 19 (2022): 3099.

[13] Ouyang, X., J. Jin, G. Jin, and Z. Wang. "Low Complexity Discrete Hartley Transform Precoded OFDM for Peak Power Reduction." *Electronics Letters* 48, no. 2 (2012): 19th January.

[14] Ochiai, H., and H. Imai. "On the Distribution of Peak-to-Average Power Ratio in OFDM." *IEEE Transactions on Communications* 49, no. 9 (2001): 282–289.

[15] Wang, Z., M. Xiaoli, and G. B. Giannakis. "OFDM or Single-Carrier Block Transmissions?" *IEEE Transactions on Communications* 52, no. 3 (2004): 380–394.

[16] Michalewicz, Z., and D. B. Fogel. *How to Solve It: Modern Heuristics*. Springer, 2004.

[17] Libeskind, S. *Euclidean and Transformational Geometry*. Jones & Bartlett Learning, 2007.

[18] Wang, Z., X. Ma, and G. B. Giannakis. "OFDM or Single-Carrier Block Transmissions?" *IEEE Transactions on Communications* 52, no. 3 (2004): 380–394.

[19] Lin, Y., and S. Phoong. "BER Minimized OFDM Systems with Channel Independent Precoders." *IEEE Transactions on Signal Processing* 51, no. 9 (2003): 2369–2380.

[20] Erceg, V., K. Hari, M. Smith, C. Tappenden, J. Costa, D. Baum, and C. Bushue. "Channel Models for Fixed Wireless Applications." In *IEEE 802.16 Broadband Wireless Access Working Group*, 2001.

[21] Nee, R. V., and A. de Wild. "Reducing the Peak-to-Average Power Ratio of OFDM." In *Proceedings of 48th IEEE Vehicular Technology Conference*, 2072–2076. Ottawa, Canada, 1998.

[22] Motorola Inc. "R1-050584: EUTRA Uplink Numerology and Design." *3GPP TSG RAN WG1, Meeting 41bis*, June 2005.

[23] Sesia, S., M. P. J. Baker, and I. Toufik. *LTE, the UMTS Long Term Evolution: From Theory to Practice*. John Wiley and Sons, 2009.

Dr. Imran Ali received the B.E. in Telecommunications from Mehran University of Engineering and Technology, Pakistan, an M.Sc. degree in Electronics and Communication Engineering from Myongji University, South Korea and PhD in Telecommunications from University of South Australia. Much of his academic research has been focused on signal processing for wireless communications. He is currently an independent researcher based in Melbourne, Australia.